

Review

# Recent Advances of Transition Metal Chalcogenides as Cathode Materials for Aqueous Zinc-Ion Batteries

Ying Liu and Xiang Wu \* 

School of Materials Science and Engineering, Shenyang University of Technology, Shenyang 110870, China

\* Correspondence: wuxiang05@sut.edu.cn

**Abstract:** In recent years, advances in lithium-ion batteries (LIBs) have pushed the research of other metal-ion batteries to the forefront. Aqueous zinc ion batteries (AZIBs) have attracted much attention owing to their low cost, high capacity and non-toxic characteristics. Among various cathodes, transition metal chalcogenides (TMCs) with a layered structure are considered as suitable electrode materials. The large layer spacing facilitates the intercalation/de-intercalation of  $\text{Zn}^{2+}$  between the layers. In this mini-review, we summarize a variety of design strategies for the modification of TMCs. Then, we specifically emphasize the zinc storage capacity of the optimized electrodes. Finally, we propose the challenges and future prospects of cathode materials for high-energy AZIBs.

**Keywords:** aqueous zinc ion battery; transition metal chalcogenides; layered structure; cathode; energy storage mechanism



**Citation:** Liu, Y.; Wu, X. Recent Advances of Transition Metal Chalcogenides as Cathode Materials for Aqueous Zinc-Ion Batteries. *Nanomaterials* **2022**, *12*, 3298. <https://doi.org/10.3390/nano12193298>

Academic Editor: Henrich Frielinghaus

Received: 4 September 2022

Accepted: 20 September 2022

Published: 22 September 2022

**Publisher's Note:** MDPI stays neutral with regard to jurisdictional claims in published maps and institutional affiliations.



**Copyright:** © 2022 by the authors. Licensee MDPI, Basel, Switzerland. This article is an open access article distributed under the terms and conditions of the Creative Commons Attribution (CC BY) license (<https://creativecommons.org/licenses/by/4.0/>).

## 1. Introduction

The growing energy crisis has driven the unprecedented development of renewable clean energy [1–3]. To date, lithium-ion batteries (LIBs) are the most widely used energy storage devices. However, the scarcity of lithium resources, the inflammability of electrolytes, and high operating environment requirements limit their growth [4–7]. Rechargeable aqueous zinc ion batteries (AZIBs) are a new generation of safety batteries. They possess certain advantages in terms of abundant zinc reserves, low anode potential (−0.763 V vs. SHE) and high theoretical capacity ( $820 \text{ mAh g}^{-1}$ ) [8–11]. Therefore, AZIBs have become one of the candidates to replace LIBs. However, zinc anodes undergo dissolution–precipitation reactions with several adverse reactions, such as dendrite growth, corrosion, and by-product formation. They are inevitable during repeated plating and stripping and seriously damage the cycle life of the cells [12]. Also, divalent zinc ions possess stronger electrostatic interactions than monovalent lithium ions [13,14]. Therefore, the choice of a suitable intercalation material is the crucial to break through this challenge.

In recent years, many efforts are devoted to the exploration of cathode materials, including Prussian blue analogs, vanadium-based and manganese-based compounds, and transition metal chalcogenides (TMCs) [15–19]. Among them, Prussian blue analogs are featured by a high voltage window, but their crystal structure is unstable and prone to phase transformation [20]. The inherent low electrical conductivity and poor structural stability of V- and Mn-based materials lead to their slow electrochemical kinetics [21–23]. The electrical conductivity of TMCs is superior to that of oxides. Additionally, TMCs are characterized by a unique layer structure with large layer spacing. Their high specific surface area can provide many active sites and reduce ion transfer paths [24]. In previous reports, Naveed et al. designed the  $\text{VS}_2$  nanosheet materials as cathodes, which maintain a capacity of  $138.3 \text{ mAh g}^{-1}$  at  $0.1 \text{ A g}^{-1}$  after 500 cycles with a retention of 94.38% [25]. Kang's group summarized the Zn storage ability of various oxides, sulfides and borides [26]. The results show that the activated MnS electrode is a potential cathode material with

both high capacity and stable cycling performance. However, bulk  $\text{MoS}_2$  and  $\text{WS}_2$  materials are virtually incapable of storing zinc ions. Therefore, it is essential to improve the electrochemical performance of TMCs by effective tuning strategies.

In recent years, there have been numerous reports on TMCs-based cathode materials. Herein, we first summarize several feasible strategies for optimizing the electrode structure. Then, we discuss the electrochemical performance of TMCs cathodes for AZIBs. Lastly, we overview the advances in cathode materials and present the current challenges and prospects for constructing advanced cathodes of AZIBs.

## 2. The Electrochemical Performance of TMCs Cathodes

Two-dimensional (2D) TMCs are composed of transition metals ( $M = \text{V}, \text{Ni}, \text{Mo}, \text{W}$  and  $\text{Mn}$ , etc.) and chalcogen elements ( $X = \text{S}, \text{Se}, \text{Te}$ ) with tunable electrical properties from semiconductors to metals. They are widely studied in the field of energy storage and conversion field [24,27,28]. In addition, graphene-like 2D layered TMCs are highly advantageous for battery applications because of their large specific surface area, which can significantly increase the contact area between the active material and the electrolyte [29]. Figure 1 illustrates the crystal structures of various TMCs materials. Their non-bonding properties allow the insertion of atoms, ions and molecules. The design strategies of TMCs materials mainly include defect engineering, hybridization, phase modulation, and in situ electrochemical oxidation. The main focus is to widen the interlayer space, improve the electrode conductivity, and accelerate the electrochemical kinetic process. We will categorize the strategies of structural design and zinc storage capabilities of various cathode materials in the following sections.

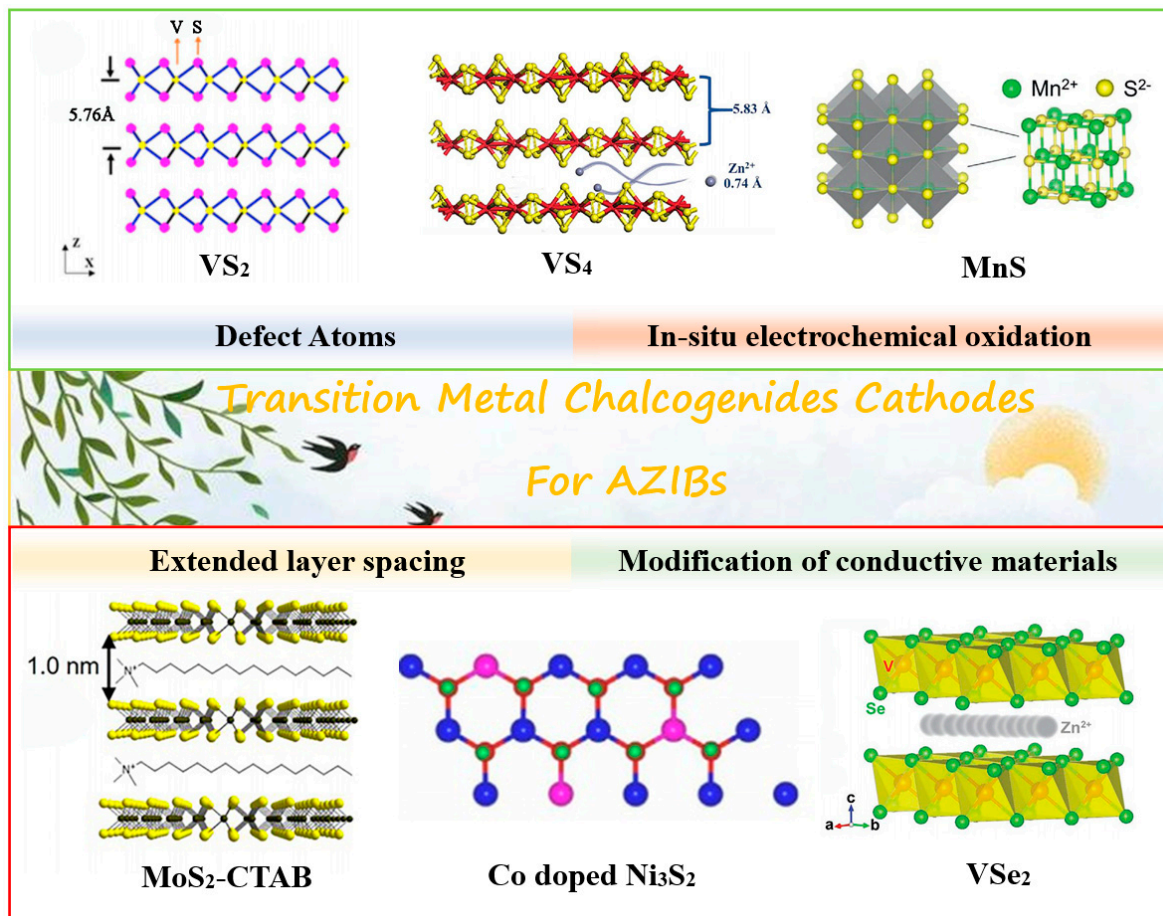


**Figure 1.** The classification of typical TMCs cathodes and the strategies of modification.

### 2.1. $VS_2$ and $VS_4$

The hexagonal-structured vanadium disulfide ( $VS_2$ ) is a member of the TMC family. It owns a layered structure with a layer spacing of 5.76 Å [30]. The S-V-S layers rely on weak van der Waals interactions (Figure 2a). Hence,  $VS_2$  materials have become an attractive host for Zn ion insertion/extraction. Nevertheless,  $VS_2$  is unstable in aqueous solutions, leading to severe capacity decay during cycling. From the aspect of modulating the material structure, coating is considered to be effective strategy. Pu et al. prepared rose-shaped  $VS_2$  encapsulated with a hydrophilic VOOH coating using a one-pot hydrothermal route [31]. The assembled cells maintained 82% capacity after 400 cycles. The rate capability and long cycle life of the optimized sample is significantly improved compared to the  $VS_2$  sample, which is attributed to the O–H in VOOH. From Figure 2b, its presence not only enhances the wetting of the electrode and electrolyte, but also prevents the dissolution of the main materials. Fan's group prepared ultrathin  $VS_2$  nanosheets grown on graphene sheets (rGO- $VS_2$ ) by a solvothermal strategy [32]. The rGO offers a large specific surface area and excellent electrical conductivity. In addition, the close contact of  $VS_2$  nanosheets with rGO can effectively prevent the dissolution and corrosion of the host materials. It ensures the high stability of the electrode in long-term cycling. Thus, Zn/rGO- $VS_2$  cells can deliver a large specific capacity (238 mAh g<sup>-1</sup> at 0.1 A g<sup>-1</sup>) and excellent rate performance (190 mAh g<sup>-1</sup> at 5 A g<sup>-1</sup>, Figure 2c). After 1000 cycles of charging and discharging, it can still maintain 93.3% of the initial capacity, as shown in Figure 2d.

The N dopant provides high affinity for the transition metals, so it is possible to form a strong coupling between the host material and the N-doped carbon. This contributes to accelerate the interfacial electron transfer and reduces cycling-induced stress and volume changes. Liu and co-workers prepared spun  $VS_2$  materials on a N-doped carbon layer ( $VS_2@N-C$ ) by an in situ hybridization strategy [33]. This strategy ensures a strong interfacial interaction between the active material and the N-doped carbon. It promotes the enhancement of electrochemical kinetics and cycling stability of the cathode. The optimal electrode possesses a capacity of 203 mAh g<sup>-1</sup> at 0.05 A g<sup>-1</sup>. Based on the Zn ion insertion and extraction mechanism, the cells can obtain a capacity of 144 mAh g<sup>-1</sup> after 600 cycles. Liu's group synthesized 1T- $VS_2$  colloidal nanospheres assembled from nanoflakes [34]. By controlling the charge cutoff voltage, a number of the Zn ions were trapped in the interlayer of the structure after the initial charge/discharge cycle. These "dead Zn" act as "pillars" to ensure the stability of the layered structure of  $VS_2$ . After 2000 cycles, the cells maintained the capacity retention of 86.7%. This unique layered structure increases the conductivity due to the presence of carbon and oxygen groups on the surface, facilitating the penetration of the aqueous electrolyte and providing more active sites.

In order to further improve the stability of  $VS_2$  electrodes in an aqueous electrolyte. Yang et al. employed an in situ electrochemical oxidation approach to enhance the interlayer space of vanadium disulfide ( $VS_2NH_3$ ) hollow spheres [35]. This large layer spacing (1.21 nm) is favorable to the improvement of zinc ion storage capacity. The  $VS_2NH_3$  samples transform into a porous structured  $V_2O_5 \cdot nH_2O$  phase during the first charging cycle (Figure 2e). It enhances the active sites and is conducive to a rapid electrochemical kinetic process. This derived electrode maintains a high capacity at 3 A g<sup>-1</sup> even after 2000 cycles. Similarly, Du and co-workers proposed the formation of  $VS_2/VO_x$  heterostructures by in situ electrochemical induction [36]. When the sample is charged to 1.8 V, the morphology of the composite changes from rose-like shape to sheet-like one. This structure can withstand the volume expansion caused by repeated cycles. Compared to the pure Zn- $VS_2$  cell, the Zn- $VS_2/VO_x$  one demonstrates a cycling stability of 3000 cycles at 1 A g<sup>-1</sup> with an improved working potential of 0.25 V (Figure 3a). This strategy of combining highly conductive sulfides and excellent chemically stable oxides leads to an enhancement of the Zn<sup>2+</sup> storage capacity of the  $VS_2/VO_x$  cathode.

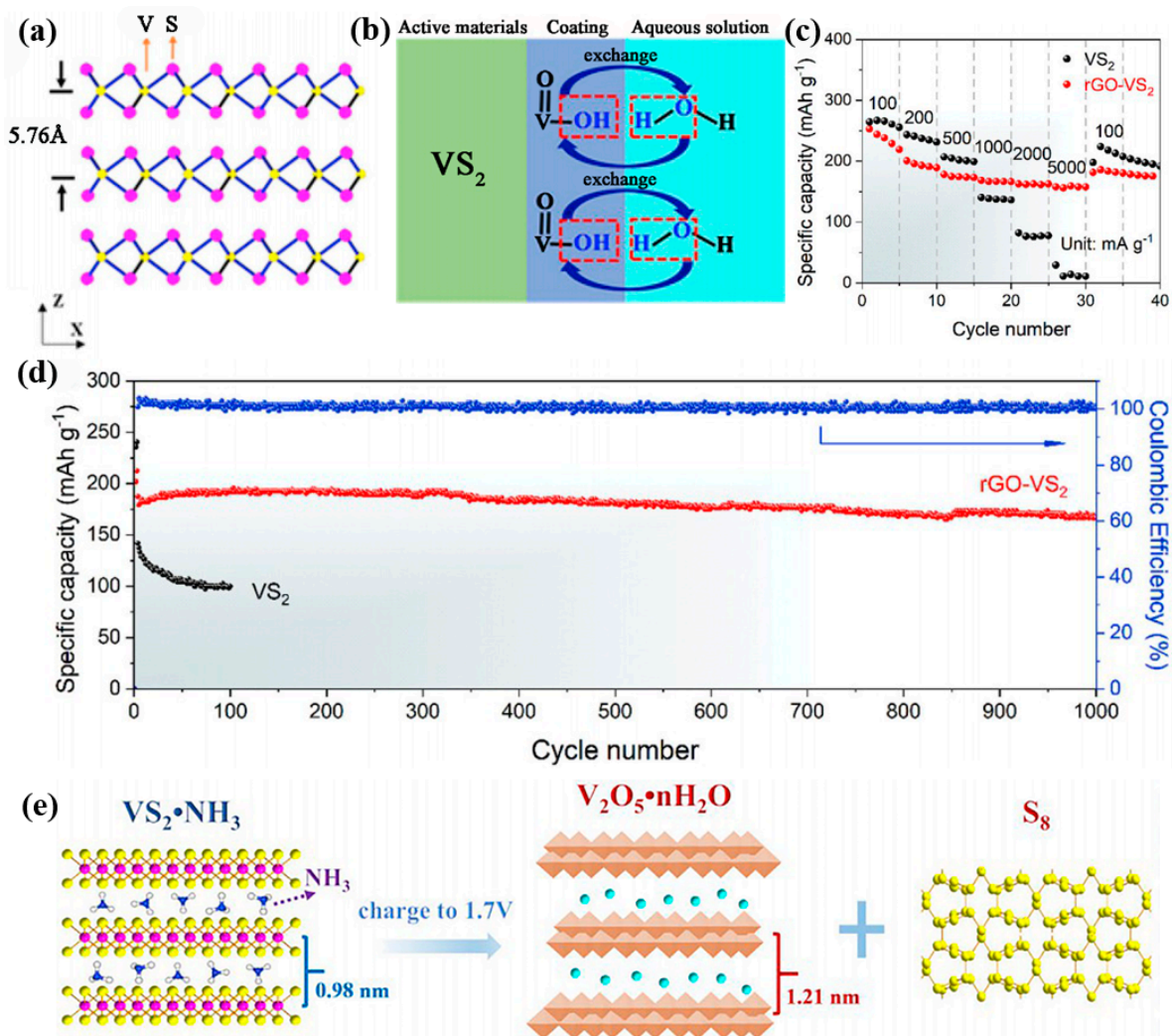


**Figure 2.** The electrochemical performance of  $\text{VS}_2$  electrodes. (a) Atomic structure of  $\text{VS}_2$  materials. (b) The working mechanism of cathode. Reproduced with permission [31]. Copyright 2019, Elsevier B.V. (c) Rate capability of  $\text{rGO-VS}_2$  and  $\text{VS}_2$ . (d) Cycling performance of these two electrodes. Reproduced with permission [32]. Copyright 2020, Elsevier B.V. (e)  $\text{Zn}^{2+}$  storage mechanism. Reproduced with permission [35]. Copyright 2021, Elsevier Inc.

$\text{VS}_4$  is a material with a one-dimensional (1D) atomic chain structure. When compared with the  $\text{VS}_2$  material, it possesses many S atoms with layer spacing up to  $5.83 \text{ \AA}$ , as shown in Figure 3b. It indicates that  $\text{VS}_4$  may show excellent zinc storage capacity. Zhu et al. prepared  $\text{VS}_4$  materials as cathodes via a hydrothermal route [37]. Density functional theory (DFT) calculations demonstrate that the electrode is capable of storing zinc ions up to a maximum specific capacity of  $262 \text{ mAh g}^{-1}$ . Then, the cell can deliver a specific capacity of  $310 \text{ mAh g}^{-1}$  at  $0.1 \text{ A g}^{-1}$ . It is higher than the theoretical capacity, which could be due to the additional absorption capacity. Furthermore, the absence of additional by-product generation suggests that the energy storage of material follows a zinc-ion embedding/deembedding mechanism. The construction of heterostructures is also an attractive strategy. In theory, the intrinsic zinc storage capacity of the cathode can be effectively enhanced by building a heterostructure with sufficient interfaces and grain boundaries. Fang's group designed  $\text{VS}_4/\text{V}_2\text{O}_3$  heterostructures with a high specific surface area [38]. The assembled battery shows a capacity of  $163 \text{ mAh g}^{-1}$  at  $0.1 \text{ A g}^{-1}$ . As a contrast, the single electrode presents inferior electrochemical performance. This demonstrates that the optimized heterogeneous material can boost the energy storage capacity.

It is also an effective strategy for improving electrochemical kinetics by compositing with highly conductive materials. Qin and co-workers synthesized  $\text{VS}_4$  composite material immobilized on reduced graphene oxide ( $\text{VS}_4/\text{rGO}$ ) as a cathode [39]. This synergistic effect enables the  $\text{VS}_4/\text{rGO}$  electrode to reach a capacity of  $180 \text{ mAh g}^{-1}$  ( $1 \text{ A g}^{-1}$ ) after 165 cycles with a capacity retention of 93.3%. Nevertheless, the above-mentioned electrochemical performance is still unsatisfactory. Chen and co-workers optimized the morphology of the  $\text{VS}_4/\text{rGO}$  composites to achieve a specific capacity of  $450 \text{ mAh g}^{-1}$  at a current density of  $0.5 \text{ A g}^{-1}$  when used as cathodes [40]. Moreover, the capacity of  $313.8 \text{ mAh g}^{-1}$  was maintained at high current densities ( $10 \text{ A g}^{-1}$ ). It indicates that the batteries possess an excellent rate capability. It is noteworthy that a new phase  $\text{Zn}_3(\text{OH})_2\text{V}_2\text{O}_7 \cdot 2\text{H}_2\text{O}$  (ZVO) appears during charging. The following reactions may occur in the electrode material:

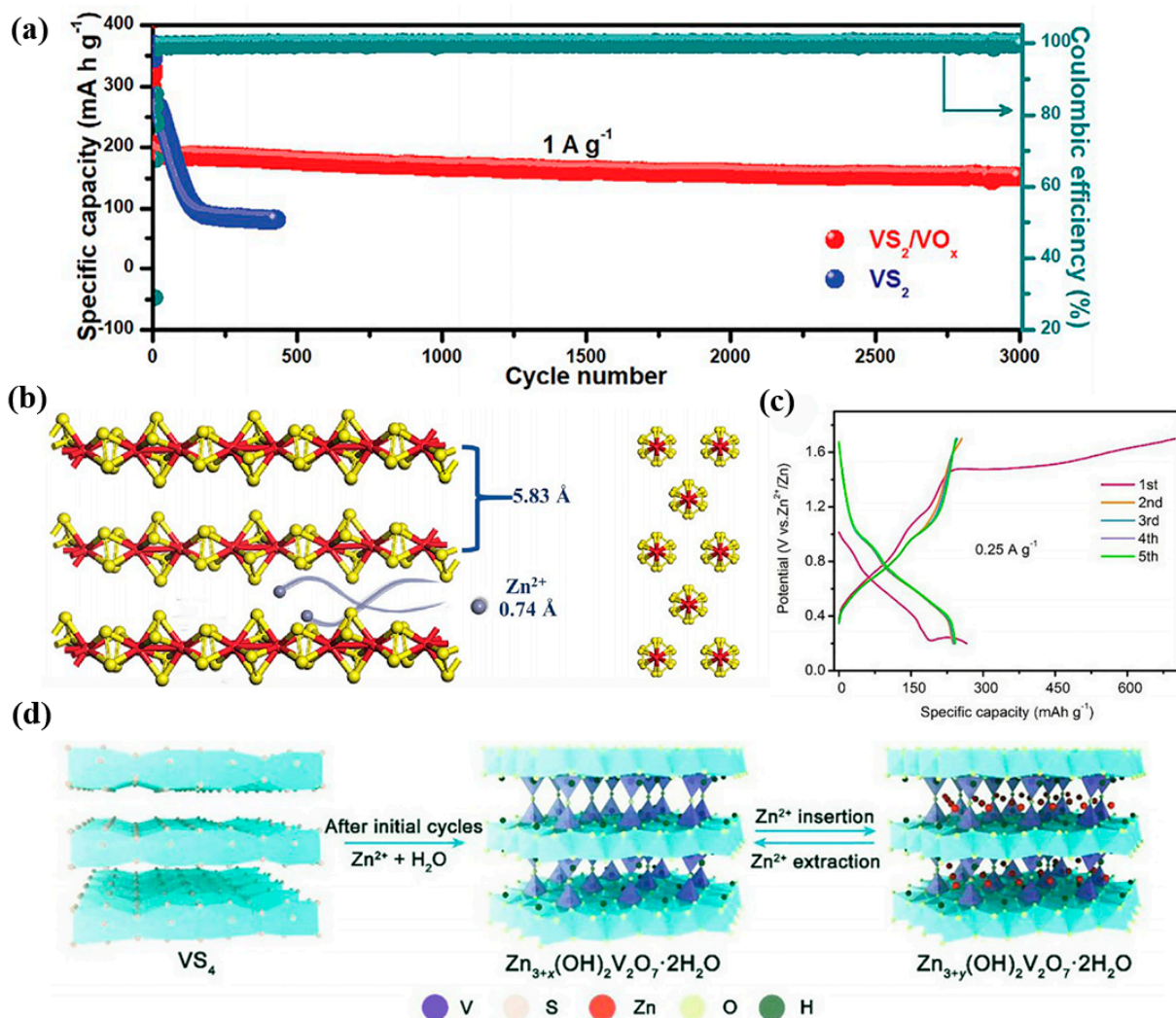
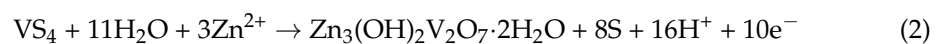


**Figure 3.** The energy storage mechanism and cycling performance. (a) The comparison of cycling performance at  $1 \text{ A g}^{-1}$ . Reproduced with permission [36]. Copyright 2020 Wiley-VCH GmbH. (b) The crystal structure of  $\text{VS}_4$  materials. Reproduced with permission [37]. Copyright 2020, The Royal Society of Chemistry. (c) The charge–discharge curves at  $0.25 \text{ A g}^{-1}$ . (d) Schematic of the energy storage mechanism of  $\text{Zn-VS}_4/\text{CNTs}$  batteries. Reproduced with permission [41]. Copyright 2021, Elsevier B.V. and Science Press.

After that, it transforms into the  $ZnV_3O_8$  phase during the long cycles, which is associated with the subsequent capacity decay. Gao et al. reported a flower-like  $VS_4$ /CNTs cathode with an abundant mesoporous structure, which effectively shortens the diffusion path of zinc ions [41]. In Figure 3c, when the first cycle is charged to 1.7 V, the charging curve undergoes a slow upward trend, which implies a phase transition process. Figure 3d further confirms that the mechanism of the phase change reaction of  $VS_4$  with zinc pyrovanadate ( $Zn_{3+x}(OH)_2V_2O_7 \cdot 2H_2O$ ). The results show that the Zn- $VS_4$ /CNTs batteries possess a reversible capacity of  $265 \text{ mAh g}^{-1}$  ( $0.25 \text{ A g}^{-1}$ ) and a good rate performance in the potential range from 0.2 to 1.7 V. Although the energy storage capacity has been significantly improved by modification of the electrode material, the inevitable phase change during the reaction process still hinders the cycle life. This may be related to the high charging voltage.

## 2.2. $MoS_2$

$MoS_2$  is a typical 2D-layered structure bound by weak van der Waals forces [42–44]. However, the ionic radius of hydrated  $Zn^{2+}$  is 0.43 nm, which places high demands on the interlayer space of the host materials. To enhance the reaction kinetics of Zn ion insertion and extraction, Li et al. extended the interlayer spacing of the (002) plane of  $MoS_2$  nanosheets from 0.62 nm to 0.70 nm [45]. Due to the addition of glucose, an amorphous carbon layer is wrapped on the surface of  $MoS_2$ . This facilitates the alleviation of volume expansion and promotes charge transfer. From Figure 4a, the specific capacity of the batteries can be maintained at  $164.5 \text{ mAh g}^{-1}$  after 600 cycles. In Figure 4b, the charge storage mechanism can be described as follow:



In addition, a flexible solid-state Zn/E- $MoS_2$  cell was further assembled using the starch/polyacrylamide (PAM) polymer electrolyte. Under different mechanical strengths, the cell still can maintain a stable charge/discharge process.

Due to the diversity of coordination of Mo and S atoms,  $MoS_2$  can show a semiconductor phase with a triangular prismatic structure (2H phase) and a metallic phase with an octahedral structure (1T phase). 1T-phase  $MoS_2$  possesses higher electrical conductivity and better hydrophilicity than 2H-phase ones [46,47]. Therefore, the material is also a promising electrode for zinc storage. Huang et al. synthesized a 1T-phase  $MoS_2$  nanosheet grown directly on reduced graphene oxide (rGO) scaffolds [48]. The addition of the rGO scaffold can serve to stabilize the 1T phase and reduce the possibility of phase transition during zinc ions insertion/extraction. In addition, it can improve the electrical conductivity, thus shortening the diffusion path of zinc ions. The initial discharge capacity of the 1T- $MoS_2$ /rGO heterogeneous electrode is  $108.3 \text{ mAh g}^{-1}$ , and the cell maintains a capacity retention of 88% after repeated charge/discharges of 1000 times.

Tang's group synthesized N-doped 1T  $MoS_2$  nanoflowers assembled from ultrathin nanosheets by a one-step hydrothermal sulfidation of Mo-based organic framework (MOF) precursors [49]. The introduction of defects effectively widens the interlayer spacing and increases the number of sulfur vacancies as well as the hydrophilicity of the sample. Zn/N-doped 1T  $MoS_2$  batteries deliver a capacity of  $149.6 \text{ mAh g}^{-1}$  ( $0.1 \text{ A g}^{-1}$ ). The capacity retention is up to 89.1% after 1000 cycles at  $3 \text{ A g}^{-1}$ . Additionally, the electrochemical performance was studied for the difference in area mass loading of the electrodes. The area capacity shows an outstanding performance when the area loading reaches  $1.701 \text{ mg cm}^{-2}$ . This implies that the electrode presents excellent rate capacity even at high loadings. Liu and co-workers reported  $MoS_2$  nanosheets with different phase contents as cathode materials [50]. Among them, the  $MoS_2$  nanosheet electrode with 1T phase of content around 70% presents favorable long-term cycling stability. This indicates that the presence of metallic 1T phase favors the ion and charge transfer.

Apart from composite with conductive materials, combination with organic molecules also promotes the increase of zinc ion storage capacity. Yao et al. designed a 2D  $\text{MoS}_2/\text{C}_{19}\text{H}_{42}\text{N}^+$  (CTAB) organic–inorganic superlattice structure ( $\text{MoS}_2\text{-CTAB}$ ) as a cathode [51]. This unique structure can significantly enlarge the interlayer spacing (1.0 nm) of the host materials (Figure 4c). In addition, the stable electrode structure can accommodate the expansion and contraction of  $\text{Zn}^{2+}$  within the host structure. The loading mass of the active material is a very important parameter for the evaluation of the specific capacity and energy density of the cell. The areal capacity of the battery increases with the area mass loading in a potential window of 0.2–1.3 V. Figure 4d demonstrates the optimal adsorption position of Zn ions at the pure  $\text{MoS}_2$  and modified  $\text{MoS}_2$  electrodes by DFT calculations. In the former structure, the Zn ion prefers to adsorb at the top site of the Mo atom with a corresponding energy of  $-0.31$  eV, but the charge accumulation of adsorbed Zn with adjacent S atoms suggests a strong electrostatic interaction between Zn and the host material. In the latter one, the adsorption energy of Zn ion at the same site is  $-0.25$  eV, and the distance between Zn and its three neighboring S atoms remains almost unchanged relative to the original electrode.

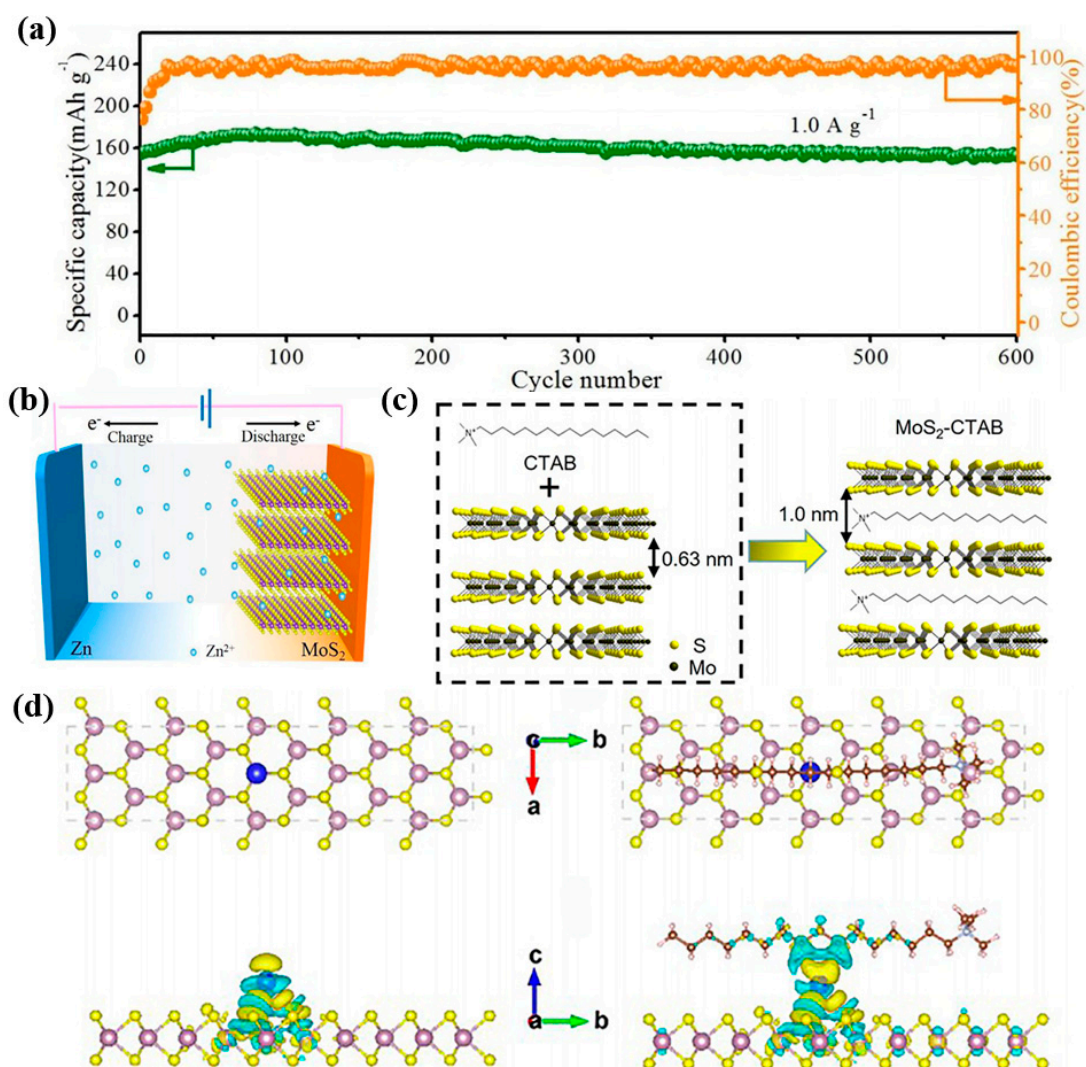


**Figure 4.** The modification of  $\text{MoS}_2$  materials and DFT calculation. (a) Cycling stability of Zn/E- $\text{MoS}_2$  batteries at  $1.0 \text{ A g}^{-1}$ . (b) Schematics of the mechanism of batteries. Reproduced with permission [45]. Copyright 2018, Elsevier B.V. (c) Schematic of the  $\text{MoS}_2\text{-CTAB}$  superlattice nanosheets and the d-spacing of the samples. (d) The charge density of pristine  $\text{MoS}_2$  and  $\text{MoS}_2\text{-CTAB}$  nanosheets during the insertion of  $\text{Zn}^{2+}$ . Reproduced with permission [51]. Copyright 2022, American Chemical Society.

### 2.3. MnS

In recent years, many efforts have been made in Mn-based oxide cathodes [52]. For instance, Minakshi et al. compared the cathodic behavior of electrolytic manganese dioxide (EMD) and chemically prepared battery-grade manganese dioxide (BGM) in a lithium hydroxide (LiOH) electrolyte [53]. The EMD cell demonstrated stable discharge/charge cycles compared to the BGM. Wang's group designed nanocrystal line structures of  $\text{MnO}_2$  materials with particle sizes typically less than 10 nm [54]. This structure confers some electrode/electrolyte contact interfaces. Therefore, the Zn/ $\text{MnO}_2$  cell delivers a capacity of 260  $\text{mAh g}^{-1}$  at 1.3 C.

However, their rate capability and cycle stability cannot meet the current high-capacity energy storage requirements. In addition, Zn ions show strong electrostatic interactions with the Mn oxide lattice, leading to large energy barriers for  $\text{Zn}^{2+}$  migration [55]. Chen et al. reported the transformation of  $\alpha$ -MnS materials into high-performance manganese oxide cathodes (MnS-EDO) by in situ electrochemical oxidation [56]. Compared to  $\alpha$ - $\text{MnO}_2$ , this electrode generated more defects and vacancies after structural reconfiguration. This indicates a rapid electrochemical kinetic process. The Zn/MnS-EDO cell shows a high specific capacity of 335.7  $\text{mAh g}^{-1}$  with capacity retention close to 100% and reversible rate performance (Figure 5a). In addition, it can undergo a repeated charge/discharge process of 4000 cycles, as shown in Figure 5b.

To further enhance the electrical conductivity of MnS, Ma and co-workers designed a MnS and rGO composite material. This synergistic effect effectively improves the Zn storage capacity of the electrode material [57]. MnS possesses various phase types:  $\alpha$ -MnS,  $\beta$ -MnS and  $\gamma$ -MnS. Both  $\beta$ - and  $\gamma$ -phases are sub-stable and readily transform to the stable rock salt structure  $\alpha$ -MnS (Figure 5c). Jiang et al. fabricated flexible zinc ion microcells with MnS as cathodes and guar gels as the quasi-solid electrolyte by etching soft templates on various substrates [58]. The cells prepared on PET substrates deliver an area-specific capacity of 178  $\mu\text{Ah cm}^{-2}$ . After 1000 cycles, they can maintain a capacity of 150  $\text{mAh g}^{-1}$  at 1  $\text{A g}^{-1}$  in Figure 5d. Moreover, the area energy density can reach 322  $\mu\text{Wh cm}^{-2}$  at a power density of 120  $\mu\text{W cm}^{-2}$ . In addition, this quasi-solid-state cell shows excellent flexibility with almost no significant capacity degradation when the device is bent at multiple angles.

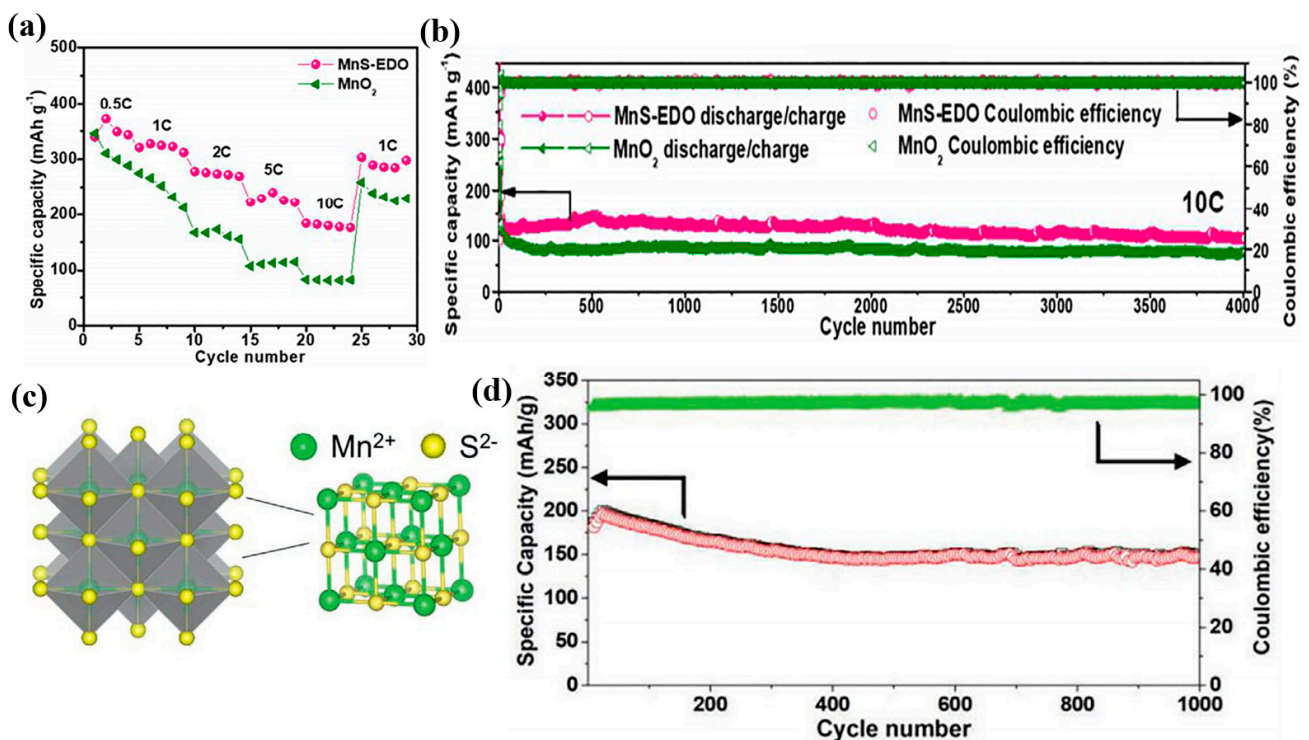


**Figure 5.** The long-term cycle performance of MnS electrodes. (a) Rate capability of the two electrode.

(b) The long-term cycling at 10 C. Reproduced with permission [56]. Copyright 2020, Elsevier Ltd. (c) Crystal structure model of  $\alpha$ -MnS; (d) Cyclic stability in 2 M ZnSO<sub>4</sub> and 0.1 M MnSO<sub>4</sub> aqueous electrolyte. Reproduced with permission [58]. Copyright 2021, Wiley-VCH GmbH.

#### 2.4. VSe<sub>2</sub>

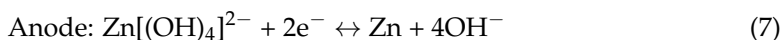
Among numerous TMCs, vanadium diselenide (VSe<sub>2</sub>) presents a typical layered structure with a sandwich-like Se–V–Se connected by van der Waals interactions [59]. The materials possess a layer spacing of 6.11 Å, which can provide sufficient transport channels and active sites for the intercalated ions [60]. Moreover, the strong electronic coupling force between adjacent V<sup>4+</sup>–V<sup>4+</sup> endows it with metallic properties. Thus, it shows great potential in terms of energy storage [61,62]. For instance, Alshareef's group explored the energy storage capacity of VSe<sub>2</sub> materials in different alkali metal batteries [63]. The morphology of VSe<sub>2</sub> nanosheets can be modulated using *N*-methylpyrrolidone (NMP) solvent, and the electrochemical performance of the samples is further improved by in situ carbon coating. The electrodes can provide a specific capacity of 768 mAh g<sup>−1</sup> (lithium storage) and 571 mAh g<sup>−1</sup> (sodium storage), respectively.

Recently, VSe<sub>2</sub> materials also show attractive performance in zinc storage. Wu et al. designed an ultrathin VSe<sub>2</sub> nanosheet as a cathode [64]. The assembled cells maintain an initial capacity of 80.8% after 500 cycles. This durable cycling stability is attributed to their fast Zn<sup>2+</sup> diffusion kinetic process and durable cycling stability. The local charge density map in Figure 6a shows a decrease in charge around the Zn ion and an increase in charge around the Se and some V sites. This demonstrates that the intercalated Zn is bonded to the Se ligand. From Figure 6b, the migration barrier for the optimal diffusion pathway of Zn ions is 0.91 eV, which corresponds to a fast ion migration rate. Based on the Zn ion insertion and extraction mechanism (Figure 6c), the cell possesses an energy density of 107.3 Wh kg<sup>−1</sup> at a power density of 81.2 W kg<sup>−1</sup>. Cai and co-workers synthesized homogeneous flower-shaped VSe<sub>2</sub> spheres using MXene as a support [65]. The specific capacity of Zn–VSe<sub>2</sub>/MXene cells was higher than the initial capacity after 2000 cycles at 5 A g<sup>−1</sup> in the voltage window of 0.2–1.6 V (Figure 6d). This may be attributed to the generation of a Zn<sub>0.25</sub>V<sub>2</sub>O<sub>5</sub> (ZVO) phase. With repeated discharge/charging, the generation and accumulation of ZVO phase provides a continuous capacity contribution to the battery.

#### 2.5. Ni<sub>3</sub>S<sub>2</sub>

Nickel sulfide (Ni<sub>3</sub>S<sub>2</sub>) is a promising electrode material with the advantages of high activity and theoretical capacity, excellent stability, and low cost [66,67]. However, Ni<sub>3</sub>S<sub>2</sub> materials perform inferiorly in cycling stability and specific capacity when they are used as a cathode for AZIBs. Structural defects are an approach to modulate the crystal structure of the materials [68]. In addition, the introduction of defects can increase the electrical conductivity and carrier density, effectively improving the electrochemical activity of the electrode materials [69].

For instance, Tong et al. doped highly reactive Co ions in Ni<sub>3</sub>S<sub>2</sub> nanocones by atomic layer deposition (ALD) and the hydrothermal method [70]. A Co12-Ni<sub>3</sub>S<sub>2</sub>/NF (C12NS) sample was used as the cathode; the hydrogel electrolyte is immersed in 5 M KOH/0.1 M Zn(AC)<sub>2</sub> solution to assemble a quasi-solid-state flexible cell. The reactivity of the electrodes is increased due to the Co doping and sulfation. The specific capacity of the activated electrode is about four times higher than that before activation. This is mainly due to the adsorption of OH radicals from the alkaline electrolyte on the sulfur sites of the Co-doped Ni<sub>3</sub>S<sub>2</sub>. The reaction mechanism can be described as:



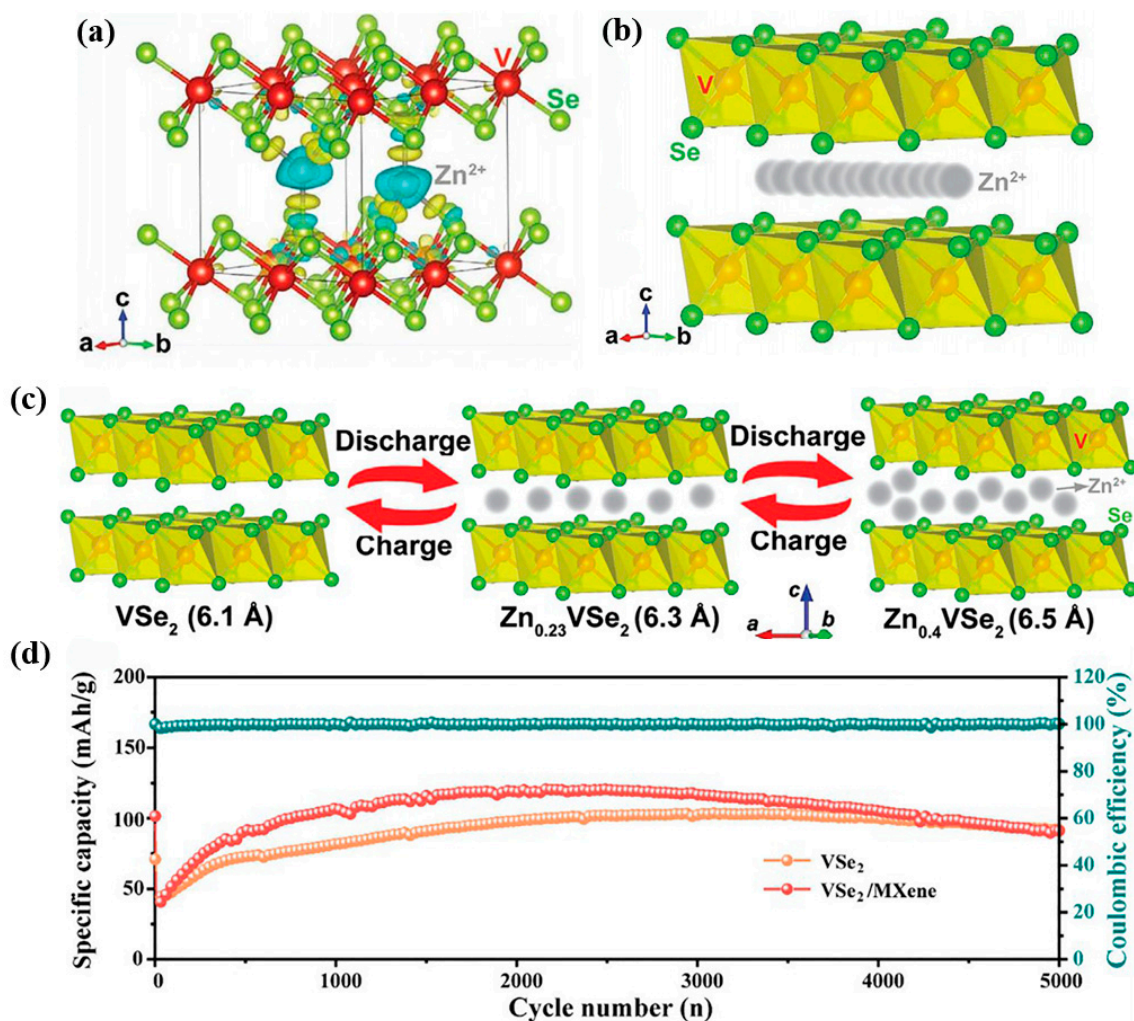


**Figure 6.** The kinetic process and cycle capability of a VSe<sub>2</sub>-based Zn battery. (a) The schematic of charge density map after zinc-ion intercalation. (b) The optimal diffusion pathway of zinc ions. (c) Schematic of the two-step Zn<sup>2+</sup> intercalation/de-intercalation process. Reproduced with permission [64]. Copyright 2020, Wiley-VCH GmbH. (d) Long-cycles performance at 5 A g<sup>-1</sup>. Reproduced with permission [65]. Copyright 2022, Elsevier Inc.

During the continuous adsorption of hydroxide radicals, sulfur and oxygen coexist. The formed oxygen–sulfur bonds enhance the electrochemical performance of the electrode material, as shown in Figure 7a. The Co-doped electrodes present a low energy barrier. It indicates that they can achieve a fast Zn ion migration (Figure 7b). In Figure 7c, the capacity retention of Co12-Ni<sub>3</sub>S<sub>2</sub>/NF electrode after 5000 cycles is up to 90%.

In addition to the defect strategy, Wang's group prepared Ni/Ni<sub>3</sub>S<sub>2</sub> nanocomposites with large specific surface areas using Ni-ZIF MOFs as precursors through a simple medium temperature solid–gas phase reaction [71]. The assembled batteries with 6 M KOH-0.6 M ZnO electrolyte possess an excellent rate capability (Figure 7d). They can maintain a capacity retention of 83% after 1000 cycles at 20 A g<sup>-1</sup> (Figure 7e). Additionally, an energy density of 379 Wh kg<sup>-1</sup> can be obtained at 340 W kg<sup>-1</sup> at a high output voltage (1.7 V). Table 1 summarizes the electrochemical performance of TMC cathodes. It can be observed that these materials present some disadvantages, mainly in terms of limited voltage window, low specific capacity and inferior cycle life. In addition, the modification tactics lead to a large difference in the electrochemical performance of the electrodes. This demonstrates that an appropriate strategy can enhance the structural stability as well as the cycle life of the cells. The VS<sub>4</sub> composite shows significant advantages with a cycle life of 3500 cycles with a stable charge/discharge process. It can be noted that the electrolytes used in these

batteries are varied. The high concentration of electrolyte contributes to the increase in capacity. Therefore, the choice of electrolyte is also crucial in future work to affect the electrochemical performance of the Zn/TMCs batteries.

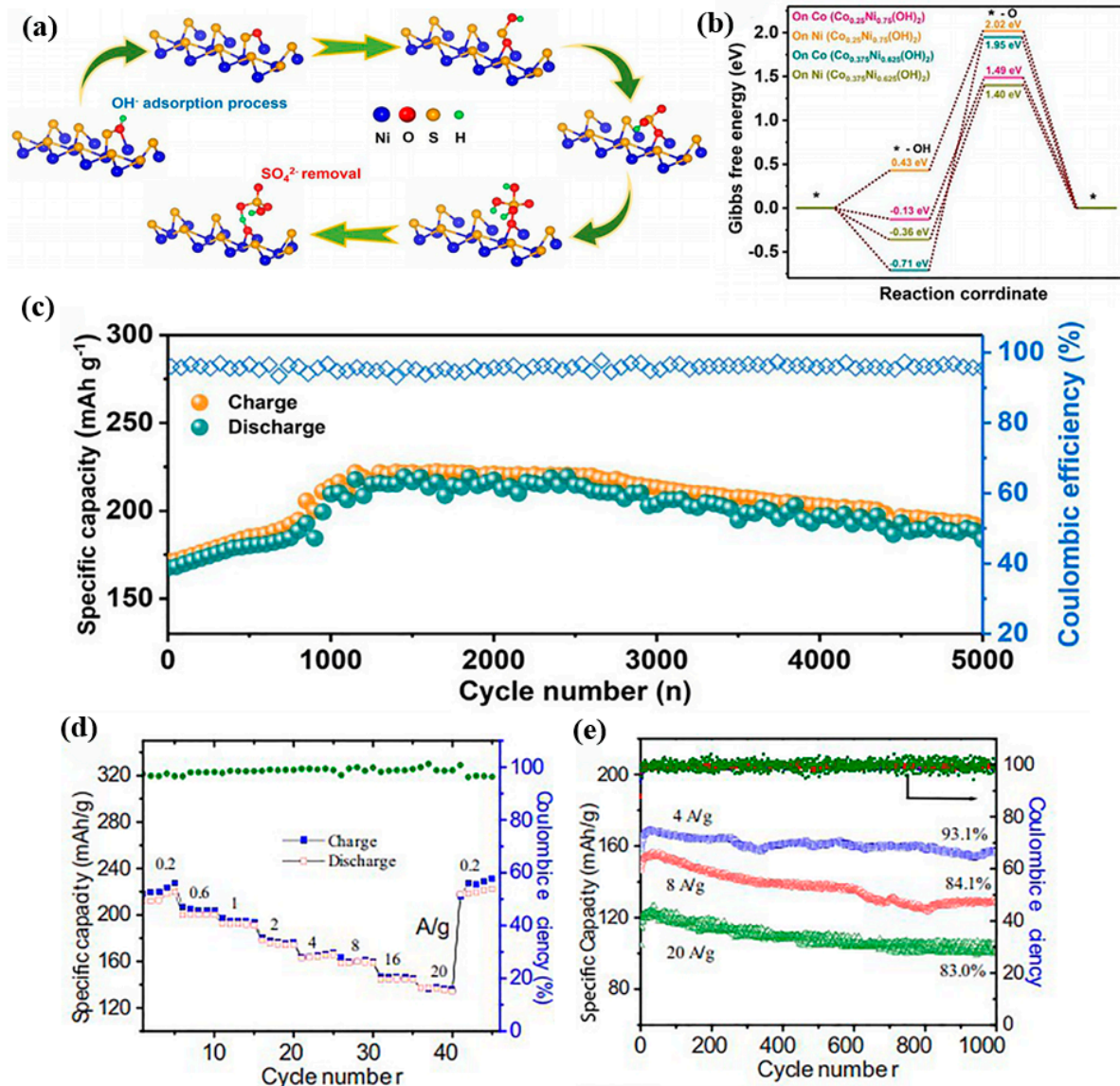


**Figure 7.** The electrochemical performance of Zn/Ni<sub>3</sub>S<sub>2</sub> batteries. (a) Schematic of nickel sulfide-adsorbing hydroxide radicals and being oxidized to form nickel hydroxide and sulfate radicals. (b) Gibbs free energies of Zn/Ni<sub>3</sub>S<sub>2</sub> batteries. (c) The cycling stability of the flexible ZC12NS battery. Reproduced with permission [70]. Copyright 2021, Elsevier B.V. and Science Press. (d) Rate capability. (e) The long-term performance. Reproduced with permission [71]. Copyright 2021, Elsevier B.V.

**Table 1.** The electrochemical performance of TMC cathodes.

| Cathodes                           | Anodes    | Voltage (V) | Electrolyte   | Capacity (mAh g <sup>-1</sup> ) | Cycle Stability (mAh g <sup>-1</sup> , Cycles, A g <sup>-1</sup> ) | Ref. |
|------------------------------------|-----------|-------------|---|---------------------------------|--|------|
| VS <sub>2</sub> @VOOH              | Zinc foil | 0.4–1.0     | 3 M ZnSO <sub>4</sub>                                 | 165 (0.1 A g <sup>-1</sup> )    | 91.4, 400, 2.5   | [31] |
| VS <sub>2</sub> and N-doped carbon | Zinc foil | 0.2–1.8     | 3 M Zn(CF <sub>3</sub> SO <sub>3</sub> ) <sub>2</sub> | 203 (0.05 A g <sup>-1</sup> )   | 144, 600, 1  | [33] |
| VS <sub>2</sub> /VO <sub>x</sub>   | Zinc foil | 0.1–1.8     | 25 M ZnCl <sub>2</sub>                                | 260 (0.1 A g <sup>-1</sup> )    | 75%, 3000, 1   | [36] |

Table 1. Cont.

| Cathodes                                       | Anodes                                  | Voltage (V) | Electrolyte   | Capacity (mAh g <sup>-1</sup> ) | Cycle Stability (mAh g <sup>-1</sup> , Cycles, A g <sup>-1</sup> ) | Ref. |
|--|---|-------------|---|---------------------------------|--|------|
| VS <sub>4</sub>                                | Zinc foil                               | 0.2–1.6     | 1 M ZnSO <sub>4</sub>                                 | 310 (0.1 A g <sup>-1</sup> )    | 110, 500, 2.5  | [37] |
| VS <sub>4</sub> /V <sub>2</sub> O <sub>3</sub> | Zinc foil                               | 0.3–1.2     | 3 M Zn(CF <sub>3</sub> SO <sub>3</sub> ) <sub>2</sub> | 163 (0.1 A g <sup>-1</sup> )    | -  | [38] |
| VS <sub>4</sub> @rGO                           | Zinc foil                               | 0–1.8       | 1 M Zn(CF <sub>3</sub> SO <sub>3</sub> ) <sub>2</sub> | 450 (0.5 A g <sup>-1</sup> )    | 82%, 3500, 10  | [40] |
| MoS <sub>2</sub>                               | Deposited zinc on carbon cloth Zn anode | 0.5–1.5     | 2 M ZnSO <sub>4</sub>                                 | 202.6 (0.1 A g <sup>-1</sup> )  | 164.5, 600, 1  | [45] |
| MoS <sub>2</sub> -CTAB                         | plated on carbon paper                  | 0.2–1.3     | 3 M ZnSO <sub>4</sub>                                 | 181.8 (0.1 A g <sup>-1</sup> )  | 92.8%, 2100, 10  | [51] |
| MnS  | zinc powder                             | 0.9–1.95    | 2 M ZnSO <sub>4</sub> and 0.1 M MnSO <sub>4</sub>     | 297 (0.1 A g <sup>-1</sup> )    | 150, 1000, 1   | [58] |
| VSe <sub>2</sub>                               | Zinc foil                               | 0.2–1.6     | 2 M ZnSO <sub>4</sub>                                 | 131.8 (0.1 A g <sup>-1</sup> )  | 80.8%, 500, 0.1  | [64] |
| Ni/Ni <sub>3</sub> S <sub>2</sub>              | Zinc foil                               | 1.3–1.9     | 6 M KOH and 0.6 M ZnO                                 | 220 (0.2 A g <sup>-1</sup> )    | 93.1%, 1000, 4   | [71] |

### 3. Summary and Outlook

AZIBs have attracted a considerable attention as an alternative to LIBs with the features of being inexpensive, environmentally friendly, resource-rich, and having high theoretical capacity. However, current cathode materials are still hampered by their inferior conductivity, slow kinetics, structural instability, and dissolution of active substances. Among them, TMCs possess a unique layered structure and a large layer spacing and high conductivity, which facilitate the transfer of ion carriers. First, the high specific surface area provides many electrochemically active sites and short ion transfer paths. Secondly, its excellent electrical conductivity ensures fast electron transfer. Finally, the open-layer structure favors the embedding of electrolyte ions and reduces the volume change. We summarized the research advances of TMCs as electrode materials in recent years. The main focus was on their modification strategies and the improvement of zinc storage capacity. Reasonable modification strategies are beneficial for the improvement of energy storage capability. Nevertheless, the goal of commercialization is still not reached. More efforts may be required to try to shorten this gap.

The electrochemical performance of TMCs materials, such as specific capacity and long cycle performance, still needs to be improved. There are several strategies for considering directions for this: (1) introducing defects (vacancies or doping) in electrode materials. It can add many active sites and conductivity to effectively increase the capacity of the battery. (2) Combining high conductivity and specific surface area materials such as MOFs and rGO. MOFs possess rich pore structures. The calcination of MOFs precursors is an effective method to prepare metal compound/carbon composites. (3) Expanded layer spacing. The increase of layer spacing is beneficial to the rapid shuttling of zinc ions, which can effectively improve the electrochemical kinetics.

Although some TMCs have been employed for energy storage, there are few materials with desired zinc storage capability. Therefore, it is still necessary to explore the unexploited cathode materials (Figure 8). We should place our eyes on the study of materials such as WS<sub>2</sub>, MoSe<sub>2</sub>, etc., and focus on the design of effective modification strategies. Additionally, the mechanism of electrochemical energy storage is still unclear. Advanced in situ characterization techniques are beneficial to explore the evolution of the structure of electrode materials during charging and discharging as well as elemental valence changes.

In addition, the structural stability of electrode materials is closely associated with their electrochemical performance. The cycling process may generate irreversible phase changes and side reactions, which lead to structural collapse or capacity loss. The modulation of heterogeneous interfaces may suppress the occurrence of side reactions. Finally, flexible

electronic devices have attracted much attention because of their high safety, portability, and wearable features. There are few reports related to flexible devices for AZIBs. They should focus on flexible substrates and cathodes with certain mechanical flexibility, and stable solid-state electrolytes with high ionic conductivity.

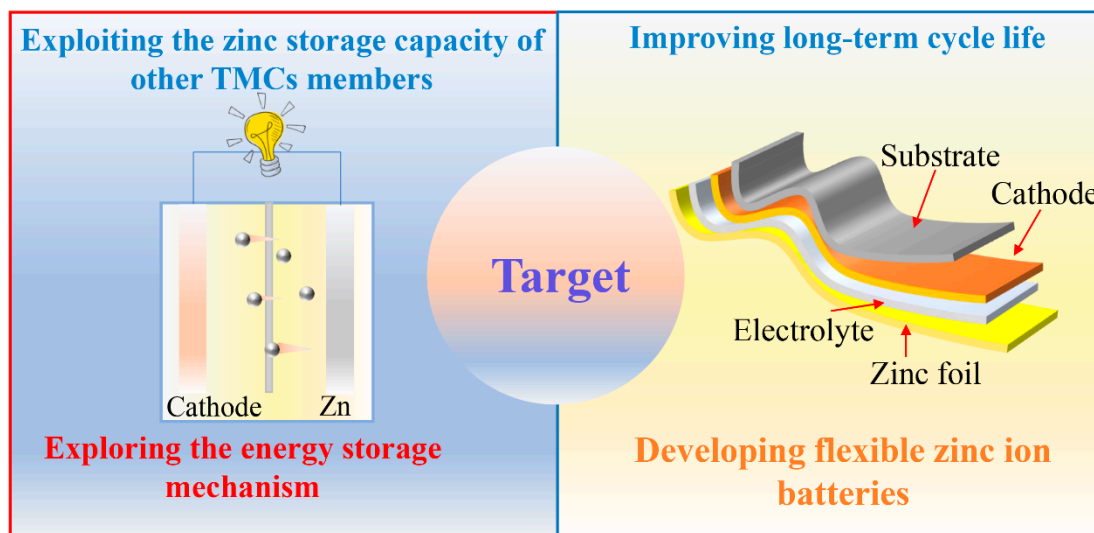


**Figure 8.** The future target of TMCs cathodes for AZIBs.

**Author Contributions:** Conceptualization, Y.L.; methodology, Y.L.; software, Y.L.; validation, Y.L.; formal analysis, Y.L.; investigation, Y.L.; resources, X.W.; data curation, Y.L. and X.W.; writing—original draft preparation, Y.L.; writing—review and editing, X.W.; visualization, Y.L.; supervision, X.W.; project administration, X.W.; funding acquisition, X.W. All authors have read and agreed to the published version of the manuscript.

**Funding:** This research was funded by National Natural Science Foundation of China (No. 52172218).

**Conflicts of Interest:** The authors declare no conflict of interest.

## References

- Goodenough, J.B. Energy storage materials: A perspective. *Energy Storage Mater.* **2015**, *1*, 158–161. [\[CrossRef\]](#)
- Zhao, D.P.; Dai, M.Z.; Zhao, Y.; Liu, H.Q.; Liu, Y.; Wu, X. Improving electrocatalytic activities of  $\text{FeCo}_2\text{O}_4/\text{FeCo}_2\text{S}_4/\text{PPy}$  electrodes by surface/interface regulation. *Nano Energy* **2020**, *72*, 104715. [\[CrossRef\]](#)
- Ruan, P.; Liang, S.; Lu, B.; Fan, H.J.; Zhou, J. Design strategies for high-energy-density aqueous zinc batteries. *Angew. Chem. Int. Ed.* **2022**, *61*, e202200598. [\[CrossRef\]](#)
- Liu, C.; Wu, X.; Wang, B. Performance modulation of energy storage devices: A case of Ni-Co-S electrode materials. *Chem. Eng. J.* **2020**, *392*, 123651. [\[CrossRef\]](#)
- Tarascon, J.M.; Armand, M. Issues and challenges facing rechargeable lithium batteries. *Nature* **2001**, *414*, 359–367. [\[CrossRef\]](#)
- Yang, D.; Zhou, Y.; Geng, H.; Liu, C.; Lu, B.; Rui, X.; Yan, Q. Pathways towards high energy aqueous rechargeable batteries. *Coord. Chem. Rev.* **2020**, *424*, 213521. [\[CrossRef\]](#)
- Ju, Z.; Zhao, Q.; Chao, D.; Hou, Y.; Pan, H.; Sun, W.; Yuan, Z.; Li, H.; Ma, T.; Su, D.; et al. Energetic Aqueous Batteries. *Adv. Energy Mater.* **2022**, *12*, 2201074. [\[CrossRef\]](#)
- Liu, Y.; Liu, Y.; Wu, X. Toward long-life aqueous zinc ion batteries by constructing stable zinc anodes. *Chem. Rec.* **2022**, e202200088. [\[CrossRef\]](#)
- Li, C.; Xie, X.; Liang, S.; Zhou, J. Issues and future perspective on zinc metal anode for rechargeable aqueous zinc-ion batteries. *Energy Environ. Mater.* **2020**, *3*, 146–159. [\[CrossRef\]](#)
- Liu, Y.; Wu, X. Hydrogen and sodium ions co-intercalated vanadium dioxide electrode materials with enhanced zinc ion storage capacity. *Nano Energy* **2021**, *86*, 106124. [\[CrossRef\]](#)
- Song, M.; Tan, H.; Chao, D.; Fan, H.J. Recent advances in Zn-ion batteries. *Adv. Funct. Mater.* **2018**, *28*, 1802564. [\[CrossRef\]](#)
- Yang, J.; Yin, B.; Sun, Y.; Pan, H.; Sun, W.; Jia, B.; Zhang, S.; Ma, T. Zinc Anode for Mild Aqueous Zinc-Ion Batteries: Challenges, Strategies, and Perspectives. *Nano-Micro Lett.* **2022**, *14*, 42. [\[CrossRef\]](#)
- Liu, Y.; Liu, Y.; Wu, X.; Cho, Y.R. Enhanced electrochemical performance of Zn/ $\text{VO}_x$  batteries by a carbon-encapsulation strategy. *ACS Appl. Mater. Interfaces* **2022**, *14*, 11654–11662. [\[CrossRef\]](#)

14. Li, H.F.; Ma, L.T.; Han, C.P.; Wang, Z.F.; Liu, Z.X.; Tang, Z.J.; Zhi, C.Y. Advanced rechargeable zinc-based batteries: Recent progress and future perspectives. *Nano Energy* **2019**, *62*, 550–587. [[CrossRef](#)]
15. Liu, Y.; Wu, X. Review of vanadium-based electrode materials for rechargeable aqueous zinc ion batteries. *J. Energy Chem.* **2021**, *56*, 223–237. [[CrossRef](#)]
16. Guo, X.; Li, J.; Jin, X.; Han, Y.; Lin, Y.; Lei, Z.; Wang, S.; Qin, L.; Jiao, S.; Cao, R. A hollow-structured manganese oxide cathode for stable Zn-MnO<sub>2</sub> batteries. *Nanomaterials* **2018**, *8*, 301. [[CrossRef](#)]
17. Liu, B. Transition metal dichalcogenides for high-performance aqueous zinc ion batteries. *Batteries* **2022**, *8*, 62. [[CrossRef](#)]
18. Trócoli, R.; La Mantia, F. An aqueous zinc-ion battery based on copper hexacyanoferrate. *ChemSusChem* **2015**, *8*, 481–485. [[CrossRef](#)]
19. Liu, Y.; Hu, P.F.; Liu, H.Q.; Wu, X.; Zhi, C.Y. Tetragonal VO<sub>2</sub> hollow nanospheres as robust cathode material for aqueous zinc ion batteries. *Mater. Today Energy* **2020**, *17*, 100431. [[CrossRef](#)]
20. Yang, Q.; Mo, F.; Liu, Z.; Ma, L.; Li, X.; Fang, D.; Chen, S.; Zhang, S.; Zhi, C. Activating C-coordinated iron of iron hexacyanoferrate for Zn hybrid-ion batteries with 10000-cycle lifespan and superior rate capability. *Adv. Mater.* **2019**, *31*, 1901521. [[CrossRef](#)]
21. Liu, Y.; Liu, Y.; Yamauchi, Y.; Allothman, Z.A.; Kaneti, Y.V.; Wu, X. Enhanced zinc ion storage capability of V<sub>2</sub>O<sub>5</sub> electrode materials with hollow interior cavities. *Batt. Supercap.* **2021**, *4*, 1867–1873. [[CrossRef](#)]
22. Zhong, Y.; Xu, X.; Veder, J.P.; Shao, Z. Self-recovery chemistry and cobalt-catalyzed electrochemical deposition of cathode for boosting performance of aqueous zinc-ion batteries. *iScience* **2020**, *23*, 100943. [[CrossRef](#)] [[PubMed](#)]
23. Liu, Y.; Liu, Y.; Wu, X.; Cho, Y.R. High performance aqueous zinc battery enabled by potassium ion stabilization. *J. Colloid Interface Sci.* **2022**, *628*, 33–40. [[CrossRef](#)] [[PubMed](#)]
24. Tan, C.; Cao, X.; Wu, X.J.; He, Q.; Yang, J.; Zhang, X.; Chen, J.; Zhao, W.; Han, S.; Nam, G.H.; et al. Recent advances in ultrathin two-dimensional nanomaterials. *Chem. Rev.* **2017**, *117*, 6225–6331. [[CrossRef](#)]
25. Naveed, A.; Yang, H.; Shao, Y.; Yang, J.; Yanna, N.; Liu, J.; Shi, S.; Zhang, L.; Ye, A.; He, B.; et al. A Highly reversible Zn anode with intrinsically safe organic electrolyte for long-cycle-life batteries. *Adv. Mater.* **2019**, *31*, 1900668. [[CrossRef](#)]
26. Liu, W.; Hao, J.; Xu, C.; Mou, J.; Dong, L.; Jiang, F.; Kang, Z.; Wu, J.; Jiang, B.; Kang, F. Investigation of zinc ion storage of transition metal oxides, sulfides, and borides in zinc ion battery systems. *Chem. Commun.* **2017**, *53*, 6872–6874. [[CrossRef](#)]
27. Liu, J.; Zhou, W.; Zhao, R.; Yang, Z.; Li, W.; Chao, D.; Qiao, S.Z.; Zhao, D. Sulfur-based aqueous batteries: Electrochemistry and strategies. *J. Am. Chem. Soc.* **2021**, *143*, 15475–15489. [[CrossRef](#)]
28. Gao, M.R.; Xu, Y.F.; Jiang, J.; Yu, S.H. Nanostructured metal chalcogenides: Synthesis, modification, and applications in energy conversion and storage devices. *Chem. Soc. Rev.* **2013**, *42*, 2986–3017. [[CrossRef](#)]
29. Gong, J.; Li, H.; Zhang, K.; Zhang, Z.; Cao, J.; Shao, Z.; Tang, C.; Fu, S.; Wang, Q.; Wu, X. Zinc-ion storage mechanism of polyaniline for rechargeable aqueous zinc-ion batteries. *Nanomaterials* **2022**, *12*, 1438. [[CrossRef](#)]
30. He, P.; Yan, M.; Zhang, G.; Sun, R.; Chen, L.; An, Q.; Mai, L. Layered VS<sub>2</sub> nanosheet-based aqueous Zn ion battery cathode. *Adv. Energy Mater.* **2017**, *7*, 1601920. [[CrossRef](#)]
31. Pu, X.; Song, T.; Tang, L.; Tao, Y.; Cao, T.; Xu, Q.; Liu, H.; Wang, Y.; Xia, Y. Rose-like vanadium disulfide coated by hydrophilic hydroxyvanadium oxide with improved electrochemical performance as cathode material for aqueous zinc-ion batteries. *J. Power Source* **2019**, *437*, 226917. [[CrossRef](#)]
32. Chen, T.; Zhu, X.; Chen, X.; Zhang, Q.; Li, Y.; Peng, W.; Zhang, F.; Fan, X. VS<sub>2</sub> nanosheets vertically grown on graphene as high-performance cathodes for aqueous zinc-ion batteries. *J. Power Source* **2020**, *477*, 228652. [[CrossRef](#)]
33. Liu, J.; Peng, W.; Li, Y.; Zhang, F.; Fan, X. A VS<sub>2</sub>@N-doped carbon hybrid with strong interfacial interaction for high-performance rechargeable aqueous Zn-ion batteries. *J. Mater. Chem. C* **2021**, *9*, 6308–6315. [[CrossRef](#)]
34. Tan, Y.; Li, S.; Zhao, X.; Wang, Y.; Shen, Q.; Qu, X.; Liu, Y.; Jiao, L. Unexpected role of the interlayer “dead Zn<sup>2+</sup>” in strengthening the nanostructures of VS<sub>2</sub> cathodes for high-performance aqueous Zn-ion storage. *Adv. Energy Mater.* **2022**, *12*, 2104001. [[CrossRef](#)]
35. Yang, M.; Wang, Z.; Ben, H.; Zhao, M.; Luo, J.; Chen, D.; Lu, Z.; Wang, L.; Liu, C. Boosting the zinc ion storage capacity and cycling stability of interlayer-expanded vanadium disulfide through in-situ electrochemical oxidation strategy. *J. Colloid Interface Sci.* **2022**, *607*, 68–75. [[CrossRef](#)]
36. Yu, D.; Wei, Z.; Zhang, X.; Zeng, Y.; Wang, C.; Chen, G.; Shen, Z.X.; Du, F. Boosting Zn<sup>2+</sup> and NH<sub>4</sub><sup>+</sup> storage in aqueous media via in-situ electrochemical induced VS<sub>2</sub>/VO<sub>x</sub> heterostructures. *Adv. Funct. Mater.* **2020**, *31*, 2008743. [[CrossRef](#)]
37. Zhu, Q.; Xiao, Q.; Zhang, B.; Yan, Z.; Liu, X.; Chen, S.; Ren, Z.; Yu, Y. VS<sub>4</sub> with a chain crystal structure used as an intercalation cathode for aqueous Zn-ion batteries. *J. Mater. Chem. A* **2020**, *8*, 10761–10766. [[CrossRef](#)]
38. Ding, J.; Gao, H.; Liu, W.; Wang, S.; Wu, S.; Fang, S.; Cheng, F. Operando constructing vanadium tetrasulfide-based heterostructures enabled by extrinsic adsorbed oxygen for enhanced zinc ion storage. *J. Mater. Chem. A* **2021**, *9*, 11433–11441. [[CrossRef](#)]
39. Qin, H.; Yang, Z.; Chen, L.; Chen, X.; Wang, L. A high-rate aqueous rechargeable zinc ion battery based on the VS<sub>4</sub>@rGO nanocomposite. *J. Mater. Chem. A* **2018**, *6*, 23757–23765. [[CrossRef](#)]
40. Chen, K.; Li, X.; Zang, J.; Zhang, Z.; Wang, Y.; Lou, Q.; Bai, Y.; Fu, J.; Zhuang, C.; Zhang, Y.; et al. Robust VS<sub>4</sub>@rGO nanocomposite as a high-capacity and long-life cathode material for aqueous zinc-ion batteries. *Nanoscale* **2021**, *13*, 12370–12378. [[CrossRef](#)]
41. Gao, S.; Ju, P.; Liu, Z.; Zhai, L.; Liu, W.; Zhang, X.; Zhou, Y.; Dong, C.; Jiang, F.; Sun, J. Electrochemically induced phase transition in a nanoflower vanadium tetrasulfide cathode for high-performance zinc-ion batteries. *J. Energy Chem.* **2022**, *69*, 356–362. [[CrossRef](#)]

42. Zhao, C.; Yu, C.; Zhang, M.; Sun, Q.; Li, S.; Banis, M.N.; Han, X.; Dong, Q.; Yang, J.; Wang, G.; et al. Enhanced sodium storage capability enabled by super wide-interlayer-spacing MoS<sub>2</sub> integrated on carbon fibers. *Nano Energy* **2017**, *41*, 66–74. [[CrossRef](#)]
43. Liu, Y.; Zhao, D.; Liu, H.; Umar, A.; Wu, X. High performance hybrid supercapacitor based on hierarchical MoS<sub>2</sub>/Ni<sub>3</sub>S<sub>2</sub> metal chalcogenide. *Chin. Chem. Lett.* **2019**, *30*, 1105–1110. [[CrossRef](#)]
44. Liang, Y.; Feng, R.; Yang, S.; Ma, H.; Liang, J.; Chen, J. Rechargeable Mg batteries with graphene-like MoS<sub>2</sub> cathode and ultrasmall Mg nanoparticle anode. *Adv. Mater.* **2011**, *23*, 640–643. [[CrossRef](#)]
45. Li, H.; Yang, Q.; Mo, F.; Liang, G.; Liu, Z.; Tang, Z.; Ma, L.; Liu, J.; Shi, Z.; Zhi, C. MoS<sub>2</sub> nanosheets with expanded interlayer spacing for rechargeable aqueous Zn-ion batteries. *Energy Storage Mater.* **2019**, *19*, 94–101. [[CrossRef](#)]
46. Jiao, Y.; Mukhopadhyay, A.; Ma, Y.; Yang, L.; Hafez, A.M.; Zhu, H. Ion transport nanotube assembled with vertically aligned metallic MoS<sub>2</sub> for high rate lithium-ion batteries. *Adv. Energy Mater.* **2018**, *8*, 1702779. [[CrossRef](#)]
47. Lei, Z.; Zhan, J.; Tang, L.; Zhang, Y.; Wang, Y. Recent development of metallic (1T) phase of molybdenum disulfide for energy conversion and storage. *Adv. Energy Mater.* **2018**, *8*, 1703482. [[CrossRef](#)]
48. Huang, M.; Mai, Y.; Fan, G.; Liang, X.; Fang, Z.; Jie, X. Toward fast zinc-ion storage of MoS<sub>2</sub> by tunable pseudocapacitance. *J. Alloys Compd.* **2021**, *871*, 159541. [[CrossRef](#)]
49. Sheng, Z.; Qi, P.; Lu, Y.; Liu, G.; Chen, M.; Gan, X.; Qin, Y.; Hao, K.; Tang, Y. Nitrogen-doped metallic MoS<sub>2</sub> derived from a metal-organic framework for aqueous rechargeable zinc-ion batteries. *ACS Appl. Mater. Interfaces* **2021**, *13*, 34495–34506. [[CrossRef](#)]
50. Liu, J.; Xu, P.; Liang, J.; Liu, H.; Peng, W.; Li, Y.; Zhang, F.; Fan, X. Boosting aqueous zinc-ion storage in MoS<sub>2</sub> via controllable phase. *Chem. Eng. J.* **2020**, *389*, 124405. [[CrossRef](#)]
51. Yao, Z.; Zhang, W.; Ren, X.; Yin, Y.; Zhao, Y.; Ren, Z.; Sun, Y.; Lei, Q.; Wang, J.; Wang, L.; et al. A volume self-regulation MoS<sub>2</sub> superstructure cathode for stable and high mass-loaded Zn-ion storage. *ACS Nano* **2022**, *16*, 12095–12106. [[CrossRef](#)] [[PubMed](#)]
52. Liu, Y.; Wu, X. Strategies for constructing manganese-based oxide electrode materials for aqueous rechargeable zinc-ion batteries. *Chin. Chem. Lett.* **2022**, *33*, 1236–1244. [[CrossRef](#)]
53. Minakshi, M.; Singh, P.; Issa, T.B.; Thurgate, S.; Marco, R.D. Lithium insertion into manganese dioxide electrode in MnO<sub>2</sub>/Zn aqueous battery. *J. Power Source* **2004**, *138*, 319–322. [[CrossRef](#)]
54. Sun, W.; Wang, F.; Hou, S.; Yang, C.; Fan, X.; Ma, Z.; Gao, T.; Han, F.; Hu, R.; Zhu, M.; et al. Zn/MnO<sub>2</sub> Battery Chemistry With H<sup>+</sup> and Zn<sup>2+</sup> Coinsertion. *J. Am. Chem. Soc.* **2017**, *139*, 9775–9778. [[CrossRef](#)] [[PubMed](#)]
55. Chao, D.; Zhou, W.; Ye, C.; Zhang, Q.; Chen, Y.; Gu, L.; Davey, K.; Qiao, S.Z. An electrolytic Zn-MnO<sub>2</sub> battery for high-voltage and scalable energy storage. *Angew. Chem. Int. Ed.* **2019**, *58*, 7823–7828. [[CrossRef](#)] [[PubMed](#)]
56. Chen, X.; Li, W.; Xu, Y.; Zeng, Z.; Tian, H.; Velayutham, M.; Shi, W.; Li, W.; Wang, C.; Reed, D.; et al. Charging activation and desulfurization of MnS unlock the active sites and electrochemical reactivity for Zn-ion batteries. *Nano Energy* **2020**, *75*, 104869. [[CrossRef](#)]
57. Ma, S.C.; Sun, M.; Sun, B.Y.; Li, D.; Liu, W.L.; Ren, M.M.; Kong, F.G.; Wang, S.J.; Guo, Z.X. In situ preparation of manganese sulfide on reduced graphene oxide sheets as cathode for rechargeable aqueous zinc-ion battery. *J. Solid State Chem.* **2021**, *299*, 122166. [[CrossRef](#)]
58. Jiang, K.; Zhou, Z.; Wen, X.; Weng, Q. Fabrications of high-performance planar zinc-ion microbatteries by engraved soft templates. *Small* **2021**, *17*, 2007389. [[CrossRef](#)]
59. Lv, R.; Robinson, J.A.; Schaak, R.E.; Sun, D.; Sun, Y.; Mallouk, T.E.; Terrones, M. Transition metal dichalcogenides and beyond: Synthesis, properties, and applications of single- and few-layer nanosheets. *Acc. Chem. Res.* **2015**, *48*, 56–64. [[CrossRef](#)]
60. Xu, K.; Chen, P.; Li, X.; Wu, C.; Guo, Y.; Zhao, J.; Wu, X.; Xie, Y. Ultrathin nanosheets of vanadium diselenide: A metallic two-dimensional material with ferromagnetic charge-density-wave behavior. *Angew. Chem. Int. Ed.* **2013**, *52*, 10477. [[CrossRef](#)]
61. Yang, C.; Feng, J.; Lv, F.; Zhou, J.; Lin, C.; Wang, K.; Zhang, Y.; Yang, Y.; Wang, W.; Li, J.; et al. Metallic graphene-like VSe<sub>2</sub> ultrathin nanosheets: Superior potassium-ion storage and their working mechanism. *Adv. Mater.* **2018**, *30*, 1800036. [[CrossRef](#)]
62. Wu, Y.; Chen, H.; Zhang, L.; Li, Q.; Xu, M.; Bao, S.J. A rough endoplasmic reticulum-like VSe<sub>2</sub>/rGO anode for superior sodium-ion capacitors. *Inorg. Chem. Front.* **2019**, *6*, 2935–2943. [[CrossRef](#)]
63. Ming, F.; Liang, H.; Lei, Y.; Zhang, W.; Alshareef, H.N. Solution synthesis of VSe<sub>2</sub> nanosheets and their alkali metal ion storage performance. *Nano Energy* **2018**, *53*, 11–16. [[CrossRef](#)]
64. Wu, Z.; Lu, C.; Wang, Y.; Zhang, L.; Jiang, L.; Tian, W.; Cai, C.; Gu, Q.; Sun, Z.; Hu, L. Ultrathin VSe<sub>2</sub> nanosheets with fast ion diffusion and robust structural stability for rechargeable zinc-ion battery cathode. *Small* **2020**, *16*, 2000698. [[CrossRef](#)]
65. Cai, S.; Wu, Y.; Chen, H.; Ma, Y.; Fan, T.; Xu, M.; Bao, S.J. Why does the capacity of vanadium selenide based aqueous zinc ion batteries continue to increase during long cycles? *J. Colloid Interface Sci.* **2022**, *615*, 30–37. [[CrossRef](#)]
66. Lin, Y.; Chen, G.; Wan, H.; Chen, F.; Liu, X.; Ma, R. 2D free-standing nitrogen-doped Ni-Ni<sub>3</sub>S<sub>2</sub>@carbon nanoplates derived from metal-organic frameworks for enhanced oxygen evolution reaction. *Small* **2019**, *15*, 1900348. [[CrossRef](#)]
67. Liu, Y.; Hu, P.; Liu, H.; Song, J.; Umar, A.; Wu, X. Toward a high performance asymmetric hybrid capacitor by electrode optimization. *Inorg. Chem. Front.* **2019**, *6*, 2824–2831. [[CrossRef](#)]
68. Zhang, Y.; Tao, L.; Xie, C.; Wang, D.; Zou, Y.; Chen, R.; Wang, Y.; Jia, C.; Wang, S. Defect engineering on electrode materials for rechargeable batteries. *Adv. Mater.* **2020**, *32*, 1905923. [[CrossRef](#)]
69. Liu, Z.; Sun, H.; Qin, L.; Cao, X.; Zhou, J.; Pan, A.; Fang, G.; Liang, S. Interlayer doping in layered vanadium oxides for low-cost energy storage: Sodium-ion batteries and aqueous zinc-ion batteries. *ChemNanoMat* **2020**, *6*, 1553–1566. [[CrossRef](#)]

70. Tong, X.; Li, Y.; Pang, N.; Zhou, Y.; Wu, D.; Xiong, D.; Xu, S.; Wang, L.; Chu, P.K. Highly active cobalt-doped nickel sulfide porous nanocones for high-performance quasi-solid-state zinc-ion batteries. *J. Energy Chem.* **2022**, *66*, 237–249. [[CrossRef](#)]
71. Wang, Q.; Liu, T.; Chen, Y.; Wang, Q. The Ni/Ni<sub>3</sub>S<sub>2</sub> nanocomposite derived from Ni-ZIF with superior energy storage performance as cathodes for asymmetric supercapacitor and rechargeable aqueous zinc ion battery. *J. Alloys Compd.* **2022**, *891*, 161935. [[CrossRef](#)]